

The shapes of galaxies in the Sloan Digital Sky Survey

Nelson D. Padilla^{1*} and Michael A. Strauss²

¹*Departamento de Astronomía y Astrofísica, Pontificia Universidad Católica de Chile, Santiago, Chile*

²*Department of Astrophysical Sciences, Princeton University, Princeton, NJ 08544 USA*

Accepted 1988 December 15. Received 2008 February 6; in original form 2008 February 6

ABSTRACT

We determine the underlying shapes of spiral and elliptical galaxies in the Sloan Digital Sky Survey Data Release 6 from the observed distribution of projected galaxy shapes, taking into account the effects of dust extinction and reddening. We assume that the underlying shapes of spirals and ellipticals are well approximated by triaxial ellipsoids. The elliptical galaxy data are consistent with oblate spheroids, with a correlation between roundness and ellipticity: the mean values of minor to middle axis ratios are 0.41 ± 0.03 for faint ellipticals and 0.76 ± 0.04 for bright ellipticals. Ellipticals show almost no dependence of axial ratio on galaxy colour, implying a negligible dust optical depth.

There is a strong variation of spiral galaxy shapes with colour indicating the presence of dust. The intrinsic shapes of spiral galaxies in the SDSS-DR6 are consistent with flat disks with a mean and dispersion of thickness to diameter ratio of $(21 \pm 5)\%$, and a face-on ellipticity, e , of $\ln(e) = -1.85 \pm 1.04$. Not including the effects of dust in the model leads to disks that are systematically rounder by $\geq 10\%$. More luminous spiral galaxies tend to have thicker and rounder disks than lower-luminosity spirals. Both elliptical and spiral galaxies tend to be rounder for larger galaxies.

The marginalised value of the edge-on r -band dust extinction E_0 in spiral galaxies is $E_0 \simeq 0.5$ magnitudes for galaxies of median colours, increasing to $E_0 = 1$ magnitudes for $g-r > 0.9$ and $E_0 > 2$ for the luminous and most compact galaxies, with half-light radii $< 2 h^{-1} \text{kpc}$.

Key words: galaxies: structure, galaxies: general, galaxies: fundamental parameters, surveys

1 INTRODUCTION

The quantitative study of intrinsic galaxy shapes started with Hubble (1930), who measured the projected axial ratios of elliptical galaxies when classifying them into what would later become the Hubble sequence. Using the projected axial ratios measured from photographic plates of 254 spiral galaxies from the Reference Catalogue of Bright Galaxies (de Vaucouleurs & de Vaucouleurs 1964), Sandage, Freeman & Stokes (1970) concluded that the disks of spiral galaxies were circular, with a disk thickness (defined as the ratio of disk height to diameter) of $\gamma = 0.25$. Later estimates from photographic plate surveys were performed by Binggeli (1980), Benacchio & Galletta (1980), and Binney & de Vaucouleurs (1981), who concluded that galactic disks were consistent with almost circular ellipses, with a mean ellipticity of $\epsilon = 0.1$. These results, based on small samples of galaxies, have been superseded in recent years by much larger studies from CCD imaging and scans of wide-field

photographic surveys (Fasano & Vio 1991). Lambas, Maddox & Loveday (1992) analyzed a sample of $\sim 13,000$ APM galaxies, and found that the distribution of ellipticities was well fitted by a one-sided Gaussian distribution centred on $\epsilon = 0$ with a dispersion of $\sigma_\epsilon = 0.13$ and a mean of $\langle \epsilon \rangle = 0.1$. Rix & Zaritsky (1995) studied a sample of kinematically selected face-on spiral galaxies in more detail, finding a typical ellipticity of $\epsilon = 0.045$ in the galactic disk potential.

Spatially resolved observations of internal kinematics can sort out the three-dimensional shape of a galaxy (Binney 1985; Franx et al. 1991; Statler 1994ab, Statler & Fry 1994; Bak & Statler 2000; Statler, Lambright, & Bak 2001). Andersen et al. (2001) and Andersen & Bershady (2003) applied this method to 24 largely face-on spirals and found a mean ellipticity of $\langle \epsilon \rangle = 0.076$, similar to that of Rix & Zaritsky. However, in both cases the selection of face-on objects may have introduced systematic biases in the sample. Future work with the SAURON spectrograph (Bacon et al. 2001; de Zeeuw et al. 2002) will allow detailed three-dimensional models to be created for a much larger number of galaxies.

Taking advantage of the large number of galaxies with

* E-mail: npadilla@astro.puc.cl

high-quality photometry and shape measurements in the Sloan Digital Sky Survey (SDSS; York et al. 2000), Ryden (2004) selected a sample of spiral galaxies from the SDSS Data Release 1 (DR1, Abazajian et al. 2003), chosen to minimise systematics due to seeing. She found that the distribution of galactic disk ellipticities can be well fit by a Gaussian distribution in $\ln \epsilon$ with a mean of -1.85 and a standard deviation of 0.89 . Vincent & Ryden (2005) extended this work using the SDSS Data Release 3 (Abazajian et al. 2005), and fit the distribution of axis ratios of both ellipticals and spirals to triaxial models. Assuming a uniform triaxiality (i.e. all galaxies are either prolate, triaxial or oblate), they found that both spiral and elliptical distributions are consistent with oblate spheroids. Moreover, high luminosity elliptical galaxies show rounder shapes than do lower-luminosity ellipticals.

Elliptical galaxies were once believed to be axisymmetric oblate spheroids, until it was discovered that their rotation velocities were insufficient to support such a geometry (Bertola & Capaccioli 1975). Binney (1976) suggested that ellipticals could be well described by a triaxial ellipsoid but Davies et al. (1983) found that small ellipticals are better fit by oblate spheroids. This variety of intrinsic shapes for elliptical galaxies makes it difficult to obtain their intrinsic shapes using only their apparent images; when this approach is used on large numbers of elliptical galaxies, it is often necessary to assume a triaxiality as in Vincent & Ryden (2005), or to use the misalignment between the internal isophotes of individual elliptical galaxies as suggested by Binney & Merrifield (1987).

Astronomers as early as Holmberg (1958) realised that the shape distribution of spiral galaxies is affected by the presence of dust. Optically thick dust obscuration aligned in the rotational plane of spirals will cause edge-on objects to appear systematically fainter, and thus they will be under-represented in magnitude-limited samples, biasing the estimates of intrinsic galaxy shapes. The dust extinction of galaxies is important for understanding the true luminosities of galaxies, the distribution of ISM in galaxies, and the relationship between optical and infrared emission from galaxies (for reviews, see Davies & Burstein 1995 and Calzetti 2001), and studies of the brightness of galaxies as a function of axial ratio should allow the effects of dust to be quantified. Valentijn (1990) studied the shapes and surface brightnesses of 16,000 galaxies from digitised photographic plates, and interpreted the data as indicating an optically thick component in disk galaxies, extending well beyond the apparent optical extent of the galaxy. Burstein, Haynes & Faber (1991) and Choloniewski (1991) however, showed that Valentijn's results were due in part to selection effects, and found that the diameters of galaxies were independent of inclination; see Davies et al. (1993) and Valentijn (1994) for further discussion of these issues. Peletier & Willmer (1992) expanded on the effects of selection biases with inclination, and emphasised that the dust opacity may depend on galaxy luminosity. Tully et al. (1998), for example, found a 1.3 mag difference in the R band between face-on and edge-on luminous galaxies, but found a negligible effect for intrinsically faint galaxies. Holwerda et al. (2005a, 2005b) used a more direct method for obtaining the opacities of spiral disks, consisting of measuring the number of field galaxies seen through galactic disks using images from the

Hubble Space Telescope WFPC2 archival data. This method had previously been applied to ground-based data by many other authors, including Zaritsky (1994), Nelson Zaritsky & Cutri (1998), and Keel & White (2001). Valotto & Giovanelli (2005) followed a different approach to derive the dust extinction in galaxies, using the inner part of the rotation curves of spiral galaxies.

More recently, a number of groups have studied the variation of galaxy properties with the inclination angle with respect to the line-of-sight, or more directly with projected galaxy shapes, to draw conclusions regarding dust extinction in spiral galaxies. Shao et al. (2007) measured dust extinction in spiral SDSS-DR2 (Abazajian et al. 2004) galaxies by studying the luminosity function of galaxies with different inclination angles, and using the intrinsic galaxy shapes as inferred from the distribution of projected axis ratios. They interpret the decrease in characteristic LF luminosity (L^*) with increasing inclination as an effect of dust extinction, where the disk optical depth is roughly proportional to the cosine of the inclination angle. However, they did not take into account the influence of dust on the projected shapes of galaxies. Unterborn & Ryden (2008) also study the variation of the luminosity function with inclination using a subsample of $\sim 78,000$ galaxies from the SDSS Data Release 6 (DR6, Adelman-McCarthy et al. 2007), finding similar results for the dependence of extinction on projected shape. They use this to define an extinction-unbiased sample of spiral galaxies for which they estimate intrinsic shapes. Even though their results indicate that these galaxies are consistent with flattened disks as was found by previous authors (e.g. Ryden 2004), the definition of the sample makes it difficult to compare their results with previous estimates. Finally, Maller et al. (2008) study the variations of galaxy properties with inclination and derive extinction corrections using the NYU-VAGC (Blanton et al. 2005), which combines data from SDSS and the Two-Micron All Sky Survey (Skrutskie et al. 2006). The median extinction over their whole sample (all morphological types) is 0.3 magnitudes in the g -band.

Dust has also been found in elliptical galaxies. Ebner, Davis & Djorgovski (1988) used colour maps to find evidence of dust in more than 30% of their sample of elliptical galaxies; $\simeq 2.5\%$ of the galaxies showed evidence for a dusty disk. However, the amount of dust in ellipticals is rather smaller than in spirals. For instance, Knapp et al. (1989) found that an elliptical galaxy contains between 1 and 10% of the dust content present in a spiral galaxy of similar luminosity (see also Leeuw et al. 2004, Krause et al. 2003, Goudfrooij 2000). Far-infrared observations of elliptical galaxies by Temi et al. (2004) also place constraints on the mass of dust in ellipticals in the range $M_{dust} = 10^5 - 10^7 h^{-1} M_\odot$, where h is the Hubble constant in units of $100 \text{ km s}^{-1} \text{ Mpc}^{-1}$.

This paper will use the SDSS DR6 to derive the intrinsic three-dimensional shapes of spiral and elliptical galaxies using the apparent photometric shapes of galaxies. We will include an in-depth analysis of the effects of dust on the distribution of apparent shapes of spiral galaxies, which will explain most of the trend seen in the distribution of spiral shapes with luminosity and colour. Our analysis weights galaxies by the inverse of the volume out to which they can be seen, thus simulating a volume-limited catalogue, and allowing us to use the full sample of galaxies available in

the SDSS DR6. Furthermore, the large number of galaxies present in this sample allows us to study the dependence of the intrinsic shapes of galaxies with luminosity, colour and physical size. Throughout this paper we assume a standard Λ CDM cosmology, with matter density parameter $\Omega_m = 0.3$ and a cosmological constant corresponding to $\Omega_\Lambda = 0.7$.

This paper is organised as follows. In Section 2 we will briefly describe the SDSS DR6 galaxies, and the parameters we consider when measuring the distribution of shapes. Section 3 explains our methodology, including our model for the effects of dust on the observed distribution of axis ratios. Section 4 shows our results, and Section 5 summarises the main conclusions drawn from this work.

2 THE SDSS GALAXY SAMPLE

We select the $\sim 585,000$ galaxies from the $r < 17.77$ magnitude-limited main spectroscopic galaxy sample of the SDSS (Strauss et al. 2002) from the SDSS DR6 (Adelman-McCarthy et al. 2007). The SDSS imaging data consist of CCD imaging data in five photometric bands (*ugriz*, Fukugita et al. 1996), taken with a drift-scan camera (Gunn et al. 1998) on a dedicated wide-field 2.5m telescope (Gunn et al. 2006). The properties of all detected objects in the images are measured (Lupton et al. 1999; Stoughton et al. 2002), and are calibrated astrometrically (Pier et al. 2003) and photometrically (Smith et al. 2002; Ivezić et al. 2004; Tucker et al. 2006). We K-correct the galaxy magnitudes using V3.2 of the code described in Blanton & Roweis (2006).

The image of each galaxy in the SDSS sample is fit to two-dimensional models of a de Vaucouleurs (1948) surface profile and an exponential profile respectively, each convolved with the PSF of the image. This fitting procedure provides a measurement of the model axial ratios (b/a) of each galaxy image in a way robust to seeing, as well as the effective radius and position angle of the galaxy. The SDSS image pipeline also fits an ellipse to the 25 mag/arcsec² isophote of each galaxy, and determines the so-called adaptive moments (Bernstein & Jarvis 2002); while the axis ratios via these statistics are generally in good agreement with those from the model fits, they are affected by seeing, and thus tend to yield systematically rounder shapes than do the model fits.

We will infer the three-dimensional shapes of spiral and elliptical galaxies separately. Park & Choi (2005) presented a very accurate way to determine SDSS galaxy morphologies using colour gradients that could be used to separate the DR6 catalogue into spiral and elliptical galaxies, but this would require analyzing the images of each individual galaxy separately. We use an alternative method: in fitting the exponential and de Vaucouleurs models, the SDSS imaging pipeline also asks for the best linear combination of these models (Abazajian et al. 2004), as quantified by the parameter *fracDev*. We use this parameter to distinguish spiral galaxies (*fracDev* < 0.8) from ellipticals (*fracDev* \geq 0.8). The axis ratios from the exponential and de Vaucouleurs models are in excellent agreement, independent of the value of *fracDev*, with a scatter of about 0.05 around the identity line, but we adopt the axis ratios from the exponential fit when *fracDev* < 0.8, and the de Vaucouleurs parameters otherwise. All our analyses are carried out using model

DeVaucouleurs or exponential *r*-band magnitudes and $g - r$ colours, depending on the galaxy type.

3 THE INTRINSIC SHAPES OF GALAXIES

In this section we will measure the distribution of projected axis ratios and present the model that will allow us to infer their intrinsic shapes.

3.1 Distributions of projected axis ratios of elliptical and spiral galaxies

Figure 1 shows distributions of spiral galaxies on the left panels, and of elliptical galaxies on the right panels. The top panels show distributions of galaxy redshifts, and the middle and lower panels the distributions of projected axis ratios. In addition, the thick solid lines in the top and middle panels show the distributions of redshifts and projected axis ratios for the full sample of galaxies in the SDSS-DR6. In these panels, the thin lines illustrate the variation of redshift and projected axis ratio distributions as the typical galaxy luminosity of the sample is increased. More luminous galaxies tend to show rounder apparent shapes (axial ratios closer to unity), suggesting that the intrinsic shapes of galaxies are a function of luminosity. This is a flux-limited sample, and thus has a strong correlation between luminosity and redshift, as shown in the top panel. With this in mind, we simulate a volume-limited measurement of apparent shapes by simply weighting each galaxy by $1/V_{max}$, where V_{max} is the volume corresponding to the maximum distance out to which a galaxy of a given apparent magnitude enters the flux-limited catalogue, taking into account K-corrections. The solid lines in the bottom panels show the resulting distributions of axial ratios for spiral and elliptical galaxies. Not surprisingly, the spiral galaxy distribution is skewed toward lower b/a values than are the ellipticals, which are rounder with b/a closer to 1.

The distribution becomes flatter when using the $1/V_{max}$ weighting. In particular, the weighted distribution of b/a values for spiral galaxies is qualitatively similar to that of Ryden (2004), who found a flat distribution over a wide range of b/a values from $b/a = 0.2$ to 0.7 for a volume limited sample of SDSS-DR2 spiral galaxies. We use $1/V_{max}$ weighting in all the analyses that follow. Galaxies fainter than $M_r - 5 \log_{10}(h) = -17$ have very small values of V_{max} , and thus tend to dominate the noise of the estimate of the distribution function; we therefore drop such low-luminosity objects in what follows. Throughout this paper, error-bars were calculated using the Jack-knife method.

We model galaxies as triaxial ellipsoids of major axis A , middle axis B , and minor axis C , parameterised by two axis ratios, C/B and B/A , and we will determine the distribution of axis ratios of the spiral and elliptical populations separately. Following Ryden (2004), we assume that the distribution of $1 - C/B$ of the three-dimensional structure can be approximated by a Gaussian with mean γ (this parameter is related to μ_γ in Ryden 2004, via $\gamma = 1 - \mu_\gamma$) and standard deviation σ_γ . We also assume that there is a log-normal distribution in the quantity $\epsilon = \log(1 - B/A)$, with mean μ and dispersion σ . Larger values of γ and μ correspond to

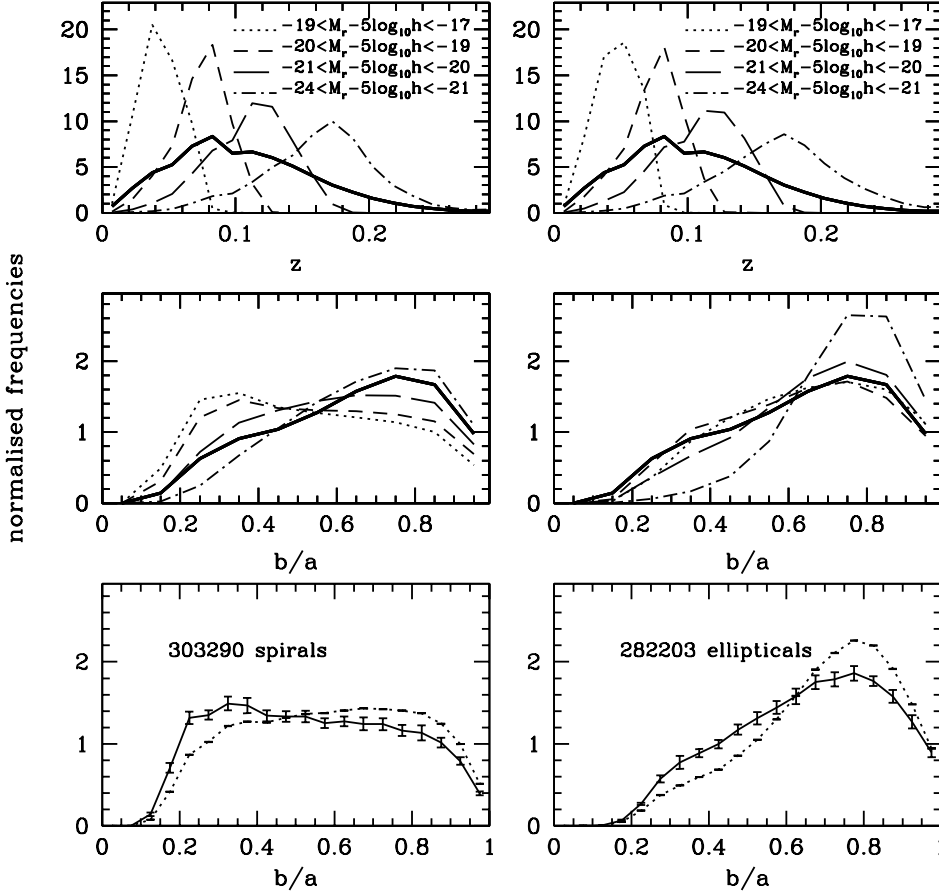


Figure 1. Left panels show distributions obtained for spiral galaxies, right panels for elliptical galaxies. Top panels: distribution of galaxy redshifts, normalised so that the area under each curve is unity. The thick solid line corresponds to all the galaxies in the SDSS-DR6. The thin lines show the distribution of axis ratios for galaxies in different bins of absolute magnitude as indicated in the key, and for spiral and elliptical galaxies separately. Middle panels: normalised distribution of axis ratios for the same samples of galaxies as in the top panels; the thick line corresponds to the full sample of galaxies. Bottom panels: Distribution of axis ratios, summed over all luminosities. The solid lines show the results when a $1/V_{max}$ weight is applied to each galaxy. The dotted lines show the results with no weighting. Errors are calculated using the Jack-knife technique.

more elliptical objects in the $B-C$ and $A-B$ planes, respectively. Given values of axis ratios drawn from these distributions, and a random viewing angle (θ, ϕ) , we compute the resulting apparent axis ratio, b/a (Binney 1985), using equations 12 – 15 from Ryden (2004). Repeating this multiple times gives a model distribution ($N_{model}(b/a)$) which can be compared directly to our measured volume-weighted distributions ($N(b/a)$).

This model assumes that the dust extinction in galaxies is independent of the viewing angle. However, we can test for the effects of dust by exploring the dependence of the shape distribution on absolute magnitude and colour. The top-left panel of Figure 2 shows the median b/a of spiral and elliptical galaxies as a function of r -band absolute magnitude. Both spiral and elliptical galaxies tend to be rounder at higher luminosities. Spiral galaxies show a change of $\Delta(b/a) \simeq 0.2$ between absolute magnitude values of $M_r - 5 \log_{10}(h) = -18.5$ and -22.5 . The variation in b/a for ellipticals is smaller, $\Delta(b/a) \simeq 0.1$.

The top-right panel shows the median b/a as a function of $g-r$ colour. Red spiral galaxies show systematically larger axis ratios than do blue spirals. We interpret the colour and

luminosity dependence of spirals as due to the reddening and dimming effects of dust, which becomes more prominent for edge-on systems. Elliptical galaxies show only a mild variation in shape with absolute magnitude, and no significant effect in colour. Thus, not unexpectedly, we see no evidence for a dust layer aligned with the principal plane of elliptical galaxies, and assume that the trend in the apparent shape of ellipticals with luminosity corresponds to a real variation of their intrinsic shapes. We study in more details the dependence of projected and intrinsic properties of spiral and elliptical galaxies in Section 4.

The middle panels of figure 2 show the luminosity and colour distribution functions (left and right panels, respectively), both estimated using the $1/V_{max}$ estimator, for spiral and elliptical galaxies. The filled circles in the middle-left panel give the r -band luminosity function estimate from Blanton et al. (2003a), with Schechter parameters $M^* - 5 \log_{10}(h) = -20.44$ and $\alpha = -1.05$; our results for the full sample (black solid lines) are in excellent agreement. As the effects of dust are more severe for edge-on objects, we also calculate the luminosity and colour functions for face-on objects ($b/a > 0.8$) only. These are shown as solid lines

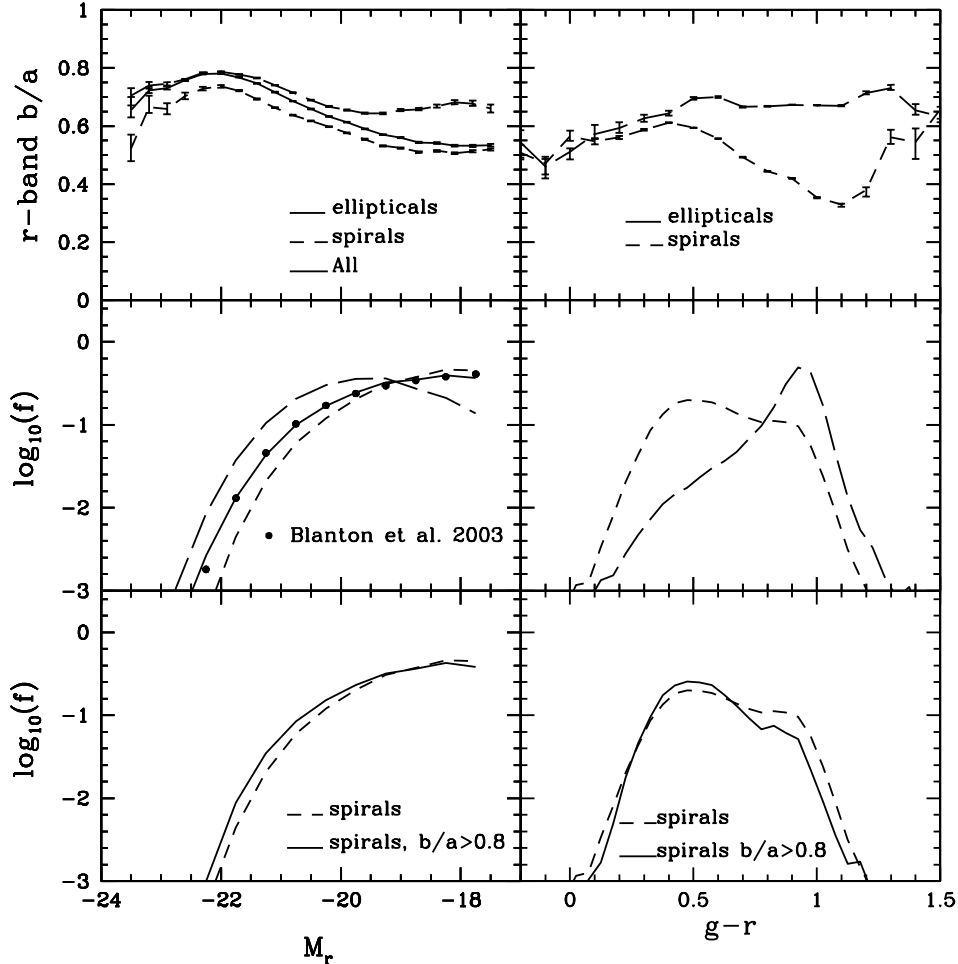


Figure 2. Top-left: median axis ratios of spiral (short dashed) and elliptical galaxies (long dashed) as a function of r -band absolute magnitude; errors are calculated using the Jack-knife technique. The middle-left panel shows the distributions of absolute magnitudes (luminosity functions) as short and long dashed lines. The filled circles show the best Schechter fit to SDSS galaxies from Blanton et al. (2003a) normalised so that the area under the curve is equal to one. The bottom-left panel shows the luminosity functions for all spiral galaxies, and for the subset of face-on spiral galaxies ($b/a > 0.8$) which we use as our unextinguished luminosity function. Right: Median axis ratio and absolute magnitude as a function of $g-r$ colour for spirals and ellipticals separately. We do not show results for the full sample to improve clarity.

for the spiral galaxies in the bottom panels of this figure; the dashed lines show the luminosity and colour functions for all the spiral galaxies for comparison. The break in the face-on luminosity function is shifted towards higher luminosities, as expected for the sample of galaxies least affected by dust. This measurement of the “unextinguished” luminosity function is in agreement with results from Shao et al. (2007), Unterborn & Ryden (2008) and, taking into account the range allowed by the analysis, with Maller et al. (2008). On the other hand, the colour function of spiral galaxies is shifted to the red due to the effects of dust. These estimates of unextinguished luminosity and unreddened colour functions will be needed when we model the effects of dust, a subject to which we now turn.

3.2 Modelling the effects of dust

In this section, we develop a simple model for the impact of a planar distribution of dust on the distribution of appar-

ent axis ratios of spiral galaxies. We assume no correlation between the dust column and the physical diameter of the galaxy, an assumption we will justify a posteriori. While Unterborn & Ryden (2008) use the inclination dependence of the luminosity function to define a sample of galaxies not affected by dust (i.e. not biased towards face-on objects), our shape fitting solves for the dust effects self-consistently.

We follow the following steps to produce the predicted distribution of projected axis ratios, given our assumed distribution of axis ratios and our measured luminosity and colour distributions:

(i) We assume that the amount of extinction and reddening are roughly proportional to the path length of the light through the galaxy. Therefore, we expect a minimum extinction when a galaxy is seen face-on, and an increasing extinction as the line-of-sight approaches the plane of the galactic disk. Similarly, Shao et al. (2007), Unterborn & Ryden (2008) and Maller et al. (2008) all find that the optical depth increases monotonically with inclination angle.

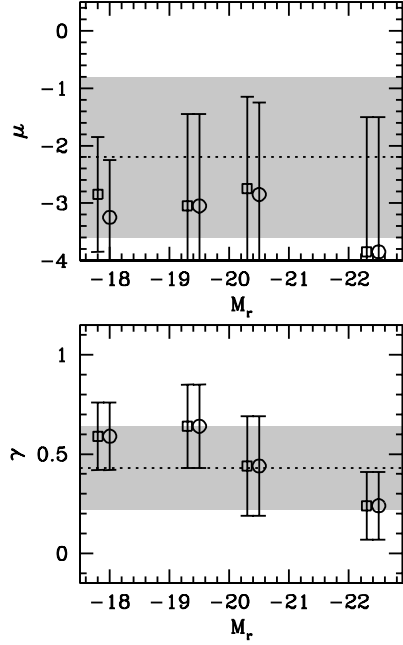


Figure 3. Dependence of the best-fitting parameters on galaxy luminosity, for elliptical galaxies. Squares represent the best fit parameters from the marginalised, one-parameter probabilities. Circles correspond to the best fit parameters in the four-dimensional parameter space. Dotted lines and shaded areas indicate the best fit parameters for the full sample of elliptical galaxies. Top panel: variations in the typical $\mu = \text{median} \log(1 - B/A)$ axis ratio; the error bars and shaded areas do not correspond to uncertainties in the parameters but indicate the best fitting width σ for the Gaussian distribution of μ values used in the model. Bottom panel: same as top panel for $\gamma = \text{median}(1 - C/B)$.

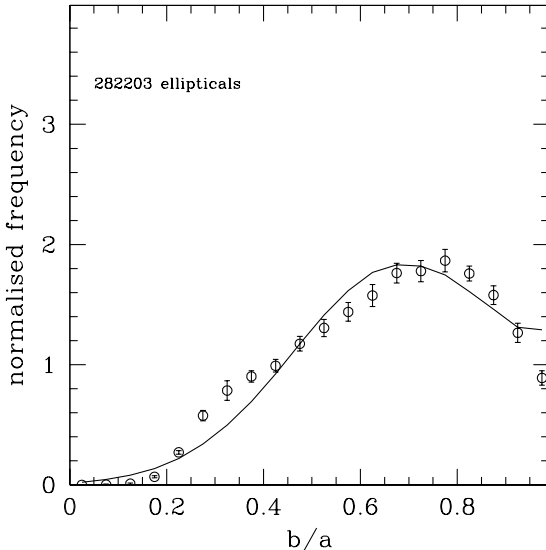


Figure 4. Comparison between the best fit model axis ratio distributions and the actual measured distributions from elliptical galaxies in the SDSS DR6. Errors are calculated using the Jack-knife technique.

The following parametrisation of the angle dependence of dust extinction is not intended as a physical model, but as a heuristic guess for the scaling. Consider an oblate triaxial galaxy with axis ratios given by $x = B/A$ and $y = C/B$. The total dust extinction as a function of inclination θ in our model is

$$E(\theta) = \begin{cases} E_0(1 + y - \cos \theta), & \text{if } \cos \theta > y \\ E_0, & \text{if } \cos \theta < y \end{cases} \quad (1)$$

where E_0 is the edge-on extinction in magnitudes in a given band and y is the galaxy height to diameter ratio extracted from a distribution of mean γ and width σ_γ . The same can be assumed for the dust reddening,

$$R(\theta) = \begin{cases} R_0(1 + y - \cos \theta), & \text{if } \cos \theta > y \\ R_0, & \text{if } \cos \theta < y \end{cases} \quad (2)$$

where R_0 is the edge-on reddening in magnitudes. In the optically thin case, which we assume here, we tie R_0 to the extinction via $E_0 = 2.77R_0$, as is appropriate for the r -band and $g - r$ colour.

(ii) We produce an extincted LF defined by

$$\phi_E(M, \theta) = \phi(M + E(\theta))$$

where $\phi(M)$ is the unextincted luminosity function calculated using only face on galaxies.

We define the ratio, f_E , between the number of observed (extincted) and intrinsic galaxies of a given luminosity $f_E(M) = \phi_E(M)/\phi(M)$. Similarly, we define $f_R(g-r)$ as the ratio between the underlying and reddened distributions of galaxy colours.

(iii) We calculate the ratio of the number of galaxies seen at inclination θ to the number expected without extinction, by multiplying the effects of reddening and extinction together,

$$\psi(\theta) = \frac{\int_{-\infty}^{\infty} \int_{-\infty}^{\infty} f_E(M) f_R(C) \phi_s(M) \phi_s(C) W(C, M) dC dM}{\int_{-\infty}^{\infty} \int_{-\infty}^{\infty} \phi_s(M) \phi_s(C) W(C, M) dM dC}, \quad (3)$$

where $C = g - r$, and the function W contains the correlation between colour and M_r . We assume that W is Gaussian with mean and dispersion extracted directly from the data; this correlation is compatible with the results shown in Figures 11 and 12 of Blanton et al. (2003b). The sub-index s indicates that the luminosity and colour functions correspond to a particular subsample of galaxies; these subsamples are defined using sharp cuts in the allowed luminosity and colour ranges. This indicates that ψ depends not only on the amount of extinction and reddening, but also on the range of luminosities and colours present in each subsample of galaxies. Note that Eq. 3 ignores the presence of large-scale structure, which is justified given the large solid angle of the SDSS sample.

(iv) We then construct the model distribution of apparent axis ratios $N_{\text{model}}(b/a)$ as described in Section 3. Rather than selecting the cosine of the viewing angle from a flat distribution, we select it from $\psi(\theta)$ as given in equation (3). In the case where $E_0 = 0$ and $R_0 = 0$, $\psi(\theta) = 1$.

In general, the effect of dust extinction and reddening is to decrease the number of galaxies seen edge-on relative to those that are face-on. This decrease depends strongly on the luminosity and colour functions, as well as on the selected range of luminosities and colours. The above process gives

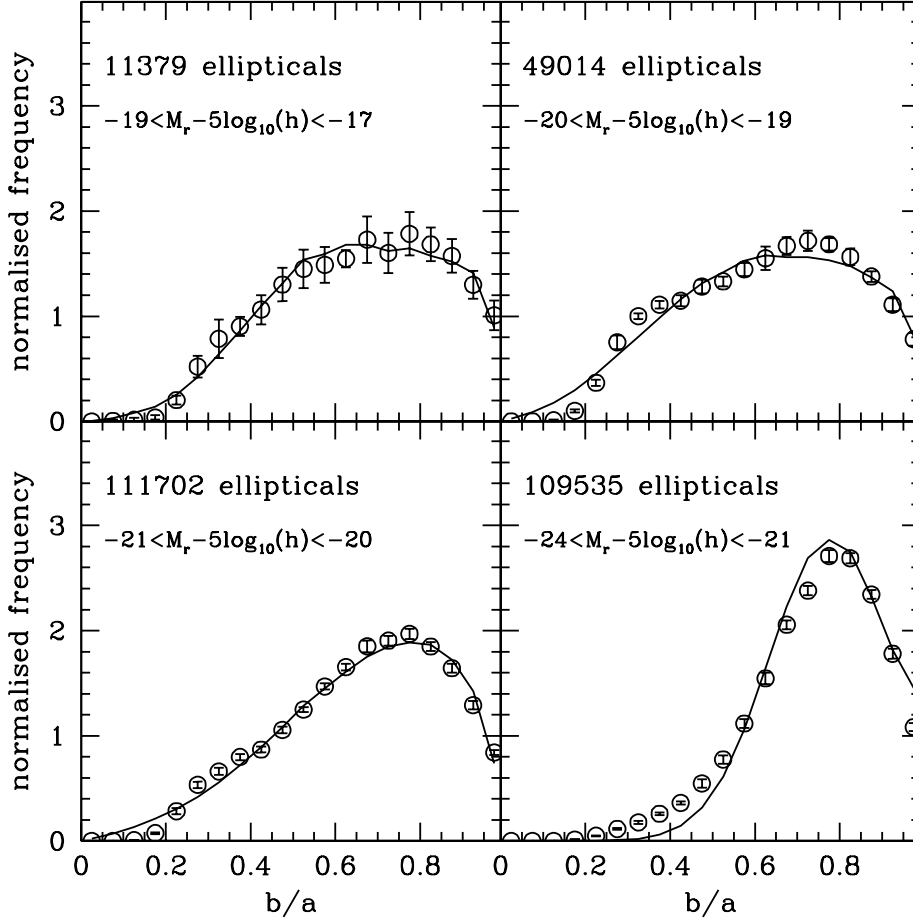


Figure 5. Comparison between the best fit model axis ratio distributions and the actual measured distributions from elliptical galaxies in the SDSS DR6 in bins of absolute magnitude. Errors are calculated using the Jack-knife technique.

a prediction for the observed projected axis ratio distribution for a given set of triaxial galaxy parameter distribution functions and dust properties. Note that for a given viewing angle, the model states that the dust affects the likelihood that a galaxy would enter the sample at that viewing angle, but does not affect the observed projected axis ratio. This is a good approximation as long as the dust is smoothly distributed within individual galaxies.

In the following section, we will constrain these parameters by fitting these predictions to the observed axis ratio distribution.

3.3 Parameter fitting

We aim to constrain the parameters μ , σ , γ and σ_γ which describe the intrinsic shapes of galaxies by fitting the observed axis ratio distribution. Spirals and ellipticals have intrinsically different shapes, and we fit to the two separately. For spirals, we also include the effects of dust via the extinction parameter E_0 which in turn defines the reddening R_0 .

We define a grid in parameter space p (four parameters for ellipticals, five for spirals). Using the parameters of each grid point p_i , we generate random three-dimensional axis ratios from the assumed distribution, observed at a random

orientation (modulated by the effects of dust, as described above). We then generate ten independent model distributions of projected axis ratios, each containing as many galaxies as the sample of galaxies under analysis. We take the average of these ten distributions as the final model distribution, $N_{\text{model}}(b/a, \{p\}_i)$, and use the jack-knife errors, $\sigma_{\text{jack-knife}}(b/a)$, obtained from the observed distribution to define a χ^2 between the real data, $N(b/a)$, and the model,

$$\chi^2(\{p\}_i) = \sum_{b/a \text{ bins}} \left(\frac{N_{\text{model}}(b/a, \{p\}_i) - N(b/a)}{\sigma_{\text{jack-knife}}(b/a)} \right)^2, \quad (4)$$

The best fit parameters correspond to the minimum value of χ^2 throughout the parameter grid. Throughout this analysis, we use a bin size of $\Delta(b/a) = 0.1$ in presenting the observed and model distributions of b/a and when calculating χ^2 .

4 RESULTS

4.1 Elliptical galaxies

The grid of parameters we used for elliptical galaxies is shown in Table 1. The number of steps for each parameter, shown in the fourth column, corresponds to a coarse initial grid; once the best fit parameters are found we re-do

Table 1. Initial parameter grid for Ellipticals

Parameter	Min. Value	Max. Value	Number of steps
μ	-4.05	-0.05	21
σ	0.4	3	18
γ	0.01	0.91	19
σ_γ	0.01	0.36	12

the analysis on a finer grid with twice the resolution centred on the best fit parameters. We repeat this refinement twice. Given the lack of colour dependence of the axis ratio distribution for ellipticals, we have assumed no dust. In order to explore the dependence of galaxy shape on luminosity, we divide the ellipticals by r -band absolute magnitude in four bins, with boundaries given by $M_r - 5\log_{10}(h) = -24, -21, -20, -19$ and -17 .

We calculate the marginalised one-parameter likelihoods (normalised to the maximum likelihood) resulting from fitting the observed $N(b/a)$. The resulting best-fit parameters are shown in Figure 3. As we guessed from the projected axis ratios, more luminous elliptical galaxies are consistent with a rounder underlying shape: the mean axis ratio γ changes from 0.4 to 0.8 with increasing luminosity. Although μ follows the opposite trend, the implied B/A three-dimensional axis ratio varies only slightly, from $\simeq 0.95$ to $\simeq 0.92$. In this figure, squares show the best-fit parameters corresponding to the marginalised one-parameter maximum likelihoods. The open symbols show the best-fit parameters as obtained from the full parameter space. In most cases, the two estimates agree reasonably well. The error bars correspond to the best fit widths, σ and σ_γ , of the distributions of $\log(1 - B/A)$ and $1 - C/B$. Table 2 shows the values of the best fit parameters for the four subsamples of elliptical galaxies, as well as the maximum likelihood value. The reduced χ^2 is ≤ 2 , indicative of a good fit, except for the highest luminosity subsample and the total sample. In these case, our simple model does not give a statistically rigorous good fit, but it still follows the shape of the observed distribution quite well. Figure 4 directly compares the observed axis ratio distribution with the model fits for the full sample of elliptical galaxies. Figure 5 shows the comparison in each bin of absolute magnitude; the agreement between the model and observed distributions, while not perfect in every case, is impressive, and thus the four-parameter model is adequate to describe the real distributions of axis ratios for the galaxy luminosities explored here.

Although Vincent & Ryden (2005) used slightly different analyses and a sample a quarter of the size the one used here, they found results in very good agreement with our own, namely that low luminosity elliptical galaxies are more consistent with prolate spheroids.

The analysis of the marginalised two-parameter likelihoods indicates that there are little or no degeneracies between the parameters used to fit the projected shapes of elliptical galaxies.

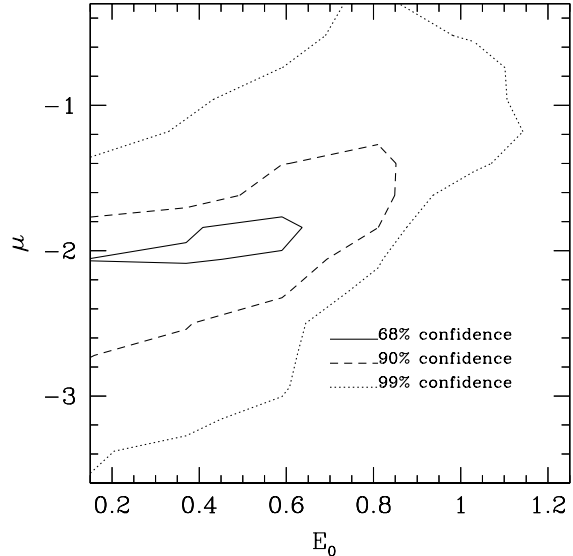


Figure 6. Marginalised likelihood contours in the μ - E_0 plane, for the full sample of spiral galaxies, corresponding to 1-, 2- and 3- σ confidence levels (shown as solid, dashed and dotted lines, respectively).

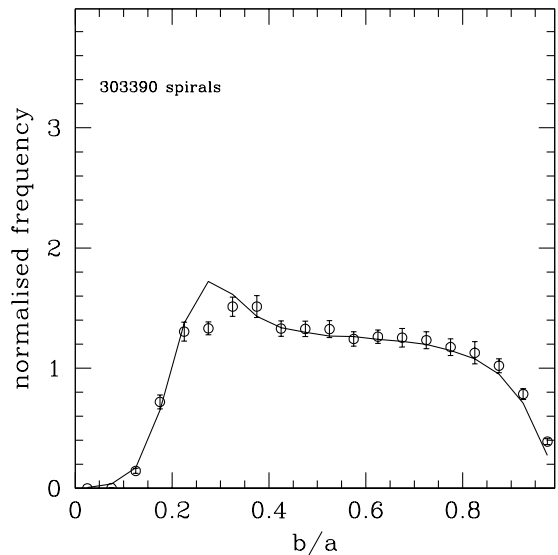


Figure 7. Comparison between the best fit model axis ratio distributions (solid line) and the actual measured distributions from the full sample of spiral galaxies in the SDSS DR6 (open symbols with error bars). Errors are calculated using the Jack-knife method.

4.2 Spiral galaxies

The distribution of spiral galaxy axis ratios depends both on absolute magnitude and colour (Figure 2), which we interpret as the effect of dust in the rotational plane of the galaxies. We model this as described in § 3.2, giving a five-parameter model. We use the grid of parameters from Table 3 to find the model quantities that best reproduce the distribution of projected spiral galaxy shapes.

Table 2. Best fit model parameters for elliptical galaxies.

Par.	Sample 1 $-17 > M_r > -19$	Sample 2 $-19 > M_r > -20$	Sample 3 $-20 > M_r > -21$	Sample 4 $-21 > M_r > -24$	All
μ	-2.85 ± 0.30	-3.05 ± 0.20	-2.75 ± 0.1	-3.85 ± 0.15	-2.2 ± 0.1
σ	1.15 ± 0.35	1.00 ± 0.05	2.60 ± 0.15	2.35 ± 0.20	1.4 ± 0.10
γ	0.41 ± 0.03	0.36 ± 0.06	0.56 ± 0.02	0.76 ± 0.04	0.57 ± 0.06
σ_γ	0.17 ± 0.03	0.21 ± 0.02	0.25 ± 0.02	0.17 ± 0.01	0.21 ± 0.02
χ^2/dof	0.41	2.0	1.72	7.2	6.8

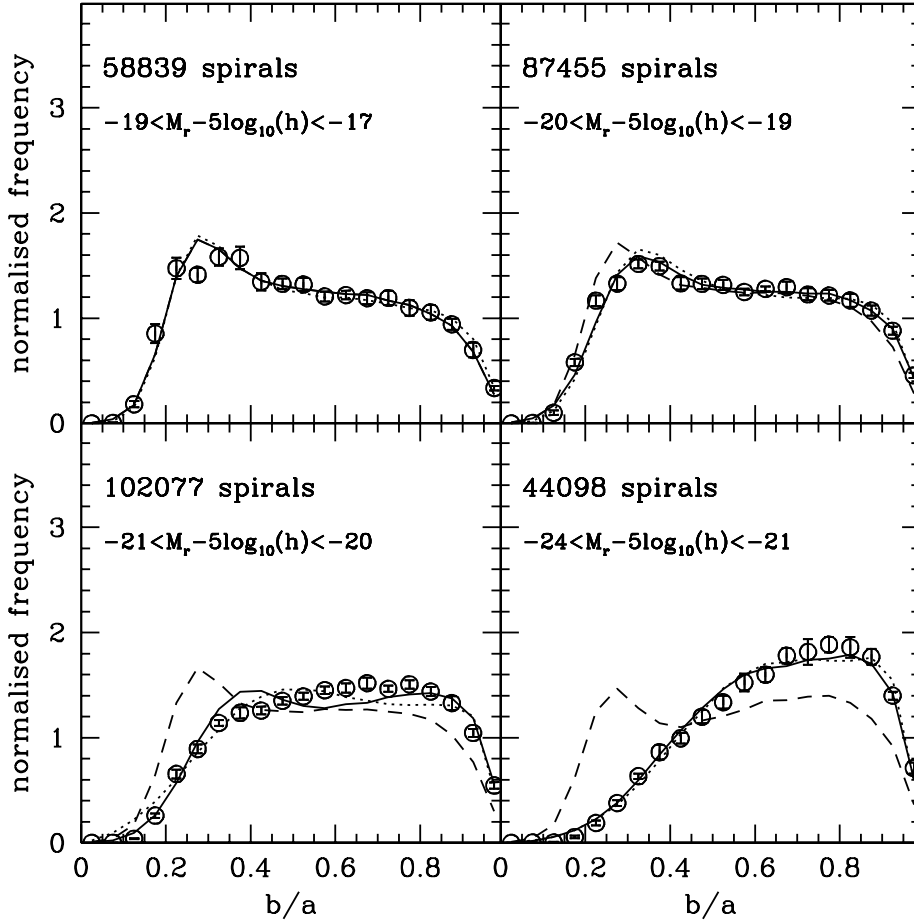


Figure 8. Comparison between the best fit model axis ratio distribution to the full sample of spiral galaxies (dashed line), and the actual measured distributions from samples of spiral galaxies with different luminosities in the SDSS DR6 (open symbols with error bars). Errors are calculated using the Jack-knife method. Solid lines show the results of fitting the model to each individual subsample including dust extinction. The dotted lines show the best fits when not including dust.

The location of the minimum χ^2 is given in Table 4; covariance between the parameters in our model explains the discrepancies with the marginalised values. As can be seen, in most cases the χ^2 values are small, which indicates the excellent agreement between the model and the data.

This corresponds to a likelihood two orders of magnitude higher than the best fit found by Ryden (2004) for the spiral galaxies in the Data Release 1 of the SDSS. Our inclusion of a dust model is only partly responsible for the improvement in the agreement between model and data; the best fit model with no dust to the full SDSS-DR6 sample of

spiral galaxies is characterised by $\chi^2 = 4.95$, only slightly higher than for the model with dust $\chi^2 = 3.83$.

It should be noted that dust extinction and the parameter μ are somewhat degenerate (none of the other parameter pairs show appreciable degeneracy). Figure 6 shows the marginalised μ vs. E_0 likelihood contours for the full sample of spiral galaxies. Interestingly, the axis ratio distribution alone allows the detection of extinction at only slightly better than 1σ . However, the strong relationship between colour and axis ratios shown in figure 2, and the results by Shao et al. (2007), Unterborn & Ryden (2008) and Maller et

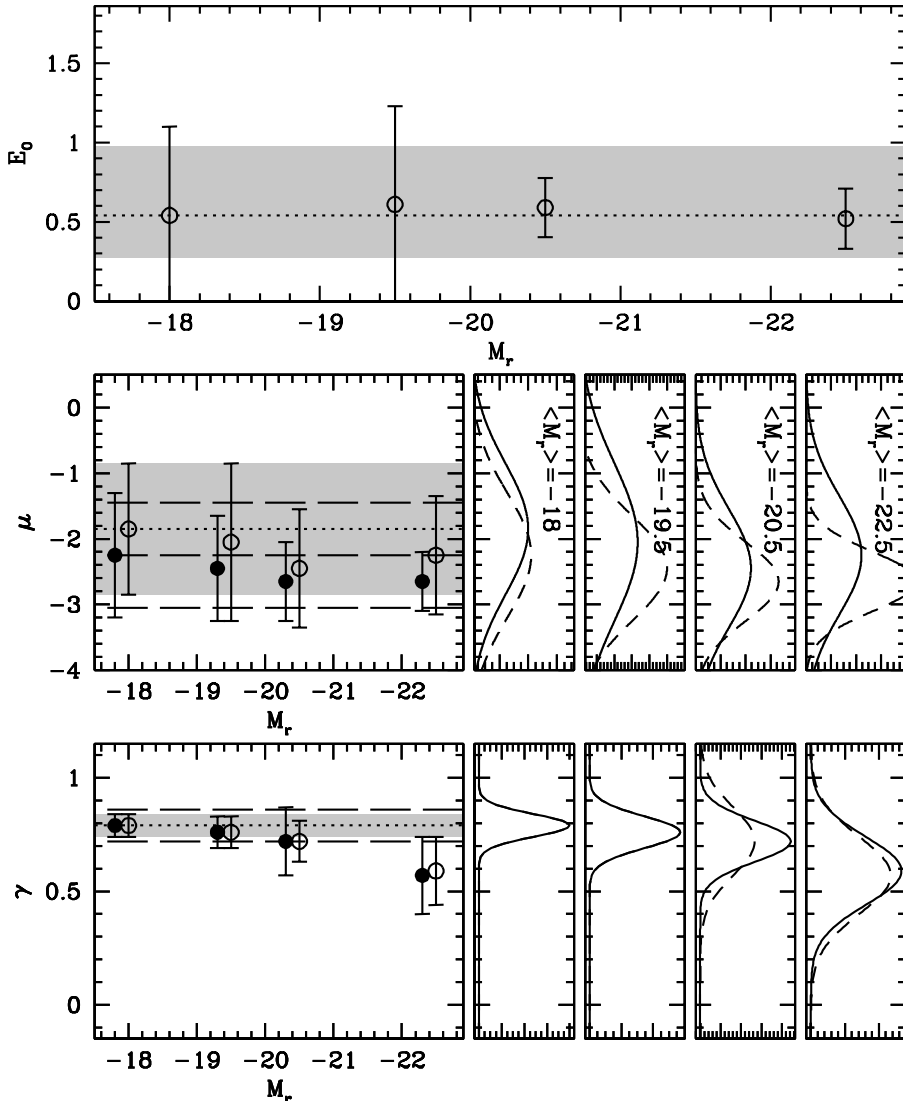


Figure 9. Dependence of the best-fitting parameters on galaxy luminosity, for spiral galaxies. Circles correspond to the best fit parameters in the five-dimensional parameter space. Open symbols show results when including dust, filled circles, results with no dust. The horizontal lines indicate the best fitting parameters obtained from the full sample of spiral galaxies (dotted lines show the best fit when including dust, thick dashed with no dust). Shaded areas and thin dashed lines show the variance in the parameters that best fit the observed distributions of projected axis ratios. Top panel: variations in the best-fitting values of extinction (filled symbols, dashed line). Error-bars show the ranges of extinction values such that the likelihood is above $\Delta\mathcal{L} = 0.36$. Middle panel: variations in the typical $\mu = \log(1 - B/A)$ axis ratio; the error bars indicate the best fitting width σ_γ for the Gaussian distribution of γ values used in the model. The corresponding distributions for each subsample are shown on the right in individual sub-panels. Bottom panel: same as middle panel for $\gamma = 1 - C/B$ (thick dashed lines are not shown to improve clarity).

al. (2008), strongly indicate the presence of dust extinction in spirals.

Figure 7 compares the observed spiral axis ratio distribution with that from our model; the two are in excellent agreement. This figure uses the full spiral sample; we have assumed that the dust and shape properties of spirals are independent of luminosity. We test that assumption in Figure 8, which shows the observed b/a distribution for spirals in different luminosity ranges, as well as the model prediction (dashed lines). The luminosity dependence in this model comes about solely from the angular selection function from equation (3) through the different ranges of luminosity that define each sample. There is excellent agreement between

the low luminosity spirals and the model; indeed, the low-luminosity subsample has a b/a distribution very close to that of the full sample, which is a consequence of our $1/V_{max}$ weighting. This agreement progressively degrades as we go towards higher luminosity. Indeed, as we saw for ellipticals, the high-luminosity spirals tend to have larger axis ratios (i.e., to be more round) than do low-luminosity objects.

There are two ways we might model this effect. A higher dust column for more luminous galaxies could preferentially remove edge-on objects from the high-luminosity bin, as suggested by Huizinga & van Albada (1992). Alternatively, as in ellipticals, there could be a direct correlation between three-dimensional shape and luminosity for spirals (e.g., Giovanelli

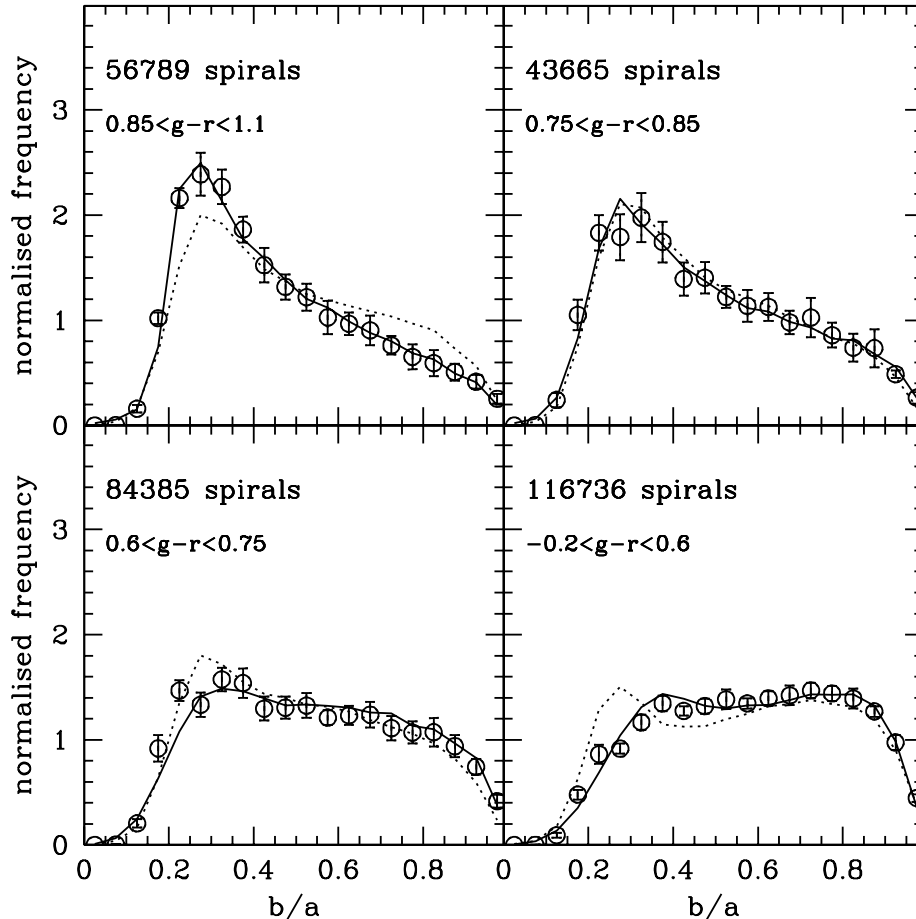


Figure 10. Comparison between the best fit model axis ratio distribution to the full sample of spiral galaxies for different $g-r$ colour cuts (dotted lines), and the actual measured distributions from samples of spiral galaxies with different $g-r$ colours in the SDSS DR6 (open symbols with error bars). Errors are calculated using the Jack-knife method. Solid lines show the results of fitting the model to each individual subsample including dust.

Table 3. Initial parameter grid for Spirals

Parameter	Min. Value	Max. Value	Number of steps
E_0	0.0	2.7	14
μ	-4.05	-0.05	21
σ	0.4	3.0	18
γ	0.01	0.91	19
σ_γ	0.01	0.36	12

et al. 1995). Indeed, there is a strong correlation between Hubble type and luminosity whereby high-luminosity spirals tend to be early types with large bulges (Roberts & Haynes 1994, Tasca & White 2005). This can explain the low number of small b/a objects at such luminosities.

We test these two options by fitting our model separately to galaxies in each range of absolute magnitude shown in Figure 8; the solid lines show the best fit distributions with E_0 as a free parameter, and the dashed lines the best fits without dust ($E_0 = 0$). Figure 9 shows the dependence of the best-fit parameters as a function of absolute mag-

nitude. The marginalised estimates are in good agreement and are not shown. Filled symbols show results with no dust, and open symbols show the results when dust extinction is taken into account. As in Figure 3, error bars indicate the $1 - \sigma$ width of the distributions in μ and γ . The sub-boxes in the middle and bottom panels show the distribution functions of x and y for each subsample in order of increasing sample luminosity from left to right; the model with dust is shown as solid lines, without dust as dashed lines. As can be seen, the main change in the inferred parameters is the value of μ , which is systematically lower when dust extinction is not considered (this is a $1 - \sigma$ effect for the full sample, and the two most luminous subsamples). The more luminous spiral galaxies show higher height to diameter ratios probably due to the presence of larger galactic bulges, and have rounder disks.

The inferred intrinsic shapes of spiral galaxies are robust to the effects of dust. The amount of extinction E_0 appears to be independent of luminosity, but the uncertainty in this parameter is large. The higher values of $\gamma \simeq 0.6$ characterising bright galaxies results in high values of projected b/a regardless of the viewing angle. This, in conjunction with

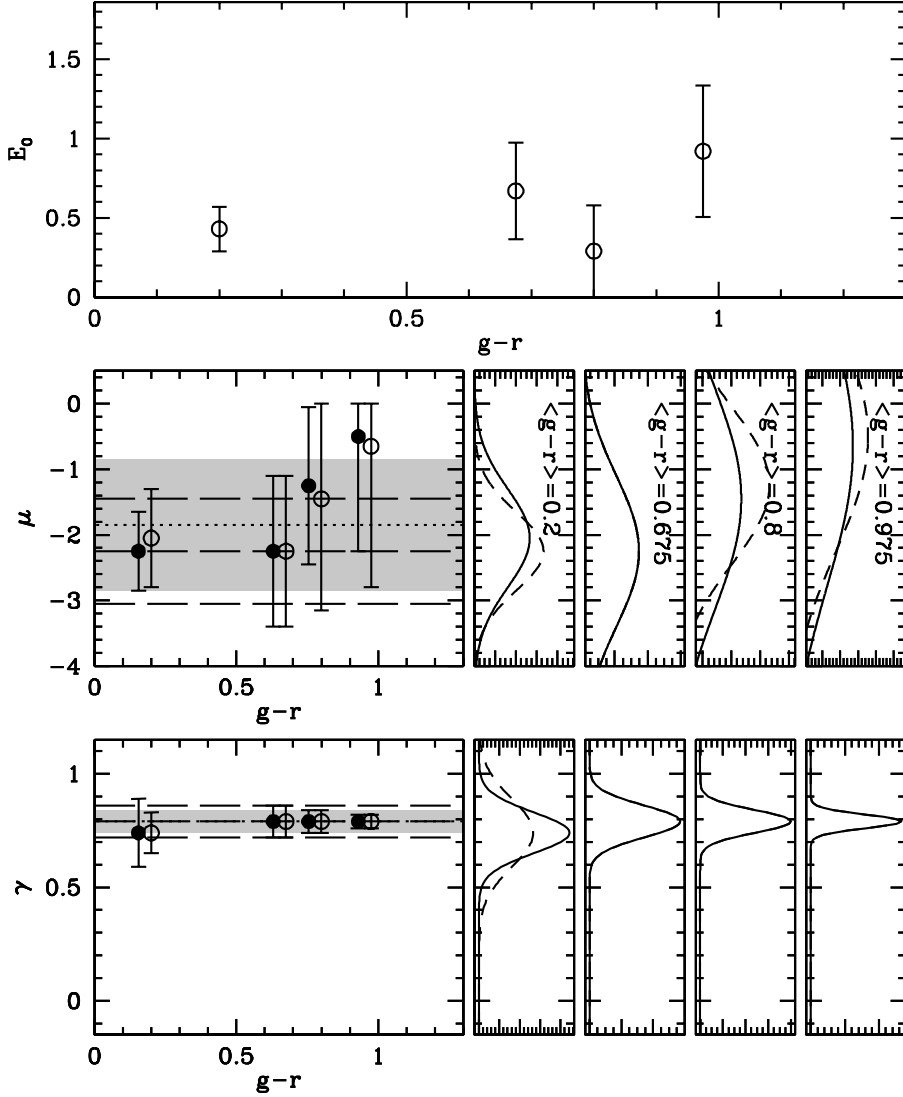


Figure 11. Dependence of the best-fitting parameters on galaxy colour, for spiral galaxies. Panels, lines and symbols are as in Figure 9.

Table 4. Best fit model parameters for spiral galaxies: Full sample and dependence on luminosity.

Par.	Sample 1 $-17 > M_r > -19$	Sample 2 $-19 > M_r > -20$	Sample 3 $-20 > M_r > -21$	Sample 4 $-21 > M_r > -24$	All
E_0	0.54 ± 0.56	0.61 ± 0.62	0.59 ± 0.19	0.52 ± 0.19	0.51 ± 0.27
μ	-1.85 ± 0.42	-2.05 ± 0.46	-2.45 ± 0.40	-2.25 ± 0.35	-1.85 ± 0.15
σ	1.03 ± 0.23	1.21 ± 0.27	0.87 ± 0.36	0.88 ± 0.35	1.04 ± 0.19
γ	0.21 ± 0.02	0.24 ± 0.03	0.28 ± 0.04	0.41 ± 0.04	0.21 ± 0.02
σ_γ	0.048 ± 0.008	0.073 ± 0.09	0.09 ± 0.02	0.15 ± 0.03	0.046 ± 0.014
χ^2/dof	1.91	2.49	7.19	2.21	3.83

the effect of extinction to reduce the number of objects seen edge-on, means that E_0 is not very well constrained from this analysis.

4.3 Axis Ratio Dependencies on Colour and Size

We now explore the different intrinsic shapes of galaxies according to their $g - r$ colour. This analysis may provide better constraints on the dust extinction in spiral galaxies. Figure 10 shows the axis ratio distribution in bins of $g - r$. The dotted lines in this figure show the model using

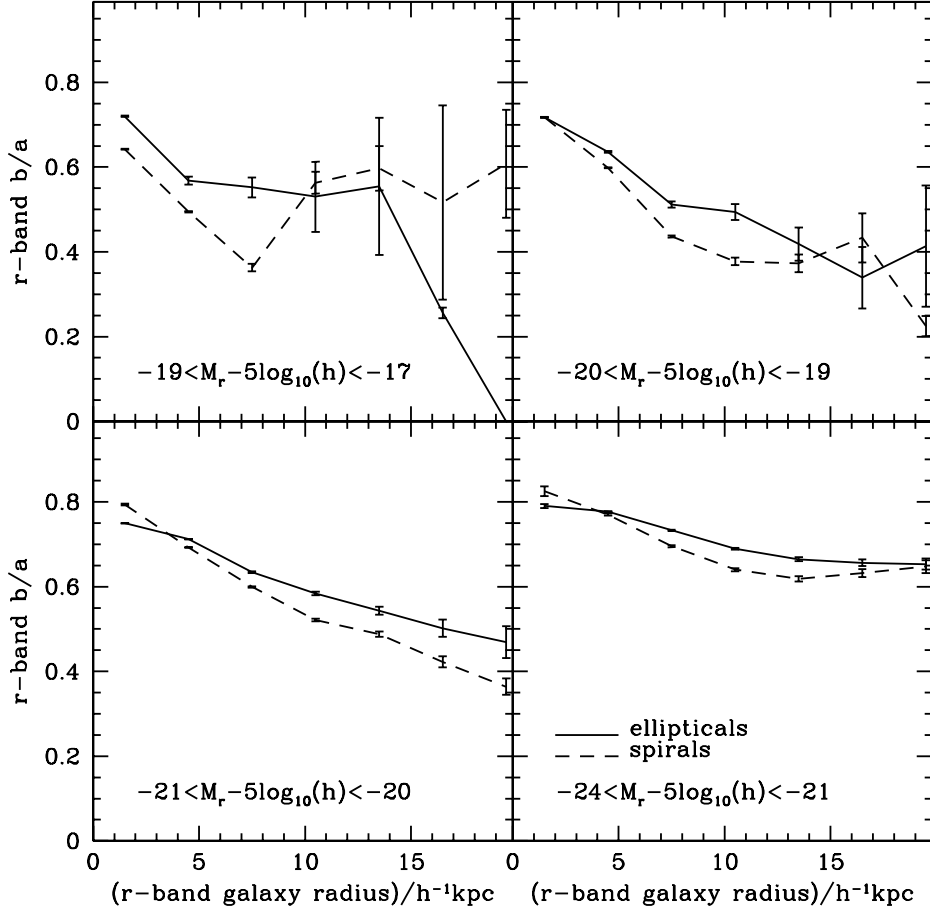


Figure 12. Variation of projected axis ratio b/a with the physical size of galaxies. Dashed lines correspond to spiral galaxies and solid lines to elliptical galaxies. Each panel corresponds to a different luminosity bin.

Table 5. Best fit model parameters for spiral galaxies: dependence on galaxy colour.

Par.	Sample 1 $0.85 < g - r < 1.1$	Sample 2 $0.75 < g - r < 0.85$	Sample 3 $0.6 < g - r < 0.75$	Sample 4 $-0.2 < g - r < 0.76$
E_0	0.9 ± 0.45	0.29 ± 0.07	0.0 ± 0.4	0.43 ± 0.15
μ	-0.65 ± 0.49	-1.45 ± 0.51	-2.25 ± 0.45	-2.05 ± 0.35
σ	2.16 ± 0.31	1.71 ± 0.22	1.15 ± 0.35	0.78 ± 0.47
γ	0.205 ± 0.02	0.205 ± 0.02	0.205 ± 0.02	0.255 ± 0.03
σ_γ	0.034 ± 0.009	0.054 ± 0.008	0.052 ± 0.016	0.09 ± 0.02
χ^2/dof	3.93	0.87	2.12	3.45

a fixed galaxy shape and dust corresponding to the best fit to the full spiral galaxy sample. The agreement is very good only for the two central ranges. Therefore, we allow the parameters to vary (solid lines), and the fit to the different colour subsamples is improved significantly. Table 5 shows the best fit parameters for each colour subsample. Figure 11 shows the resulting best fit parameters with and without dust (open and filled symbols, respectively). The intrinsic shapes of galaxies change with colour; blue galaxies tend to have rounder disks as seen face-on than red spirals (see the

trend in μ), and the inferred amount of dust extinction is consistent with an increase from $E_0 = 0.4$ for blue galaxies, to $E_0 = 1$ for the reddest sample. There are only small differences between the recovered values of μ and γ when including dust.

Up to this point we had assumed that there is no dependence of shape and dust extinction with the physical size of the galaxy. The best-fit parameter values are those appropriate for galaxies of median size within each subsample. However, the intrinsic shape and the amount of dust ex-

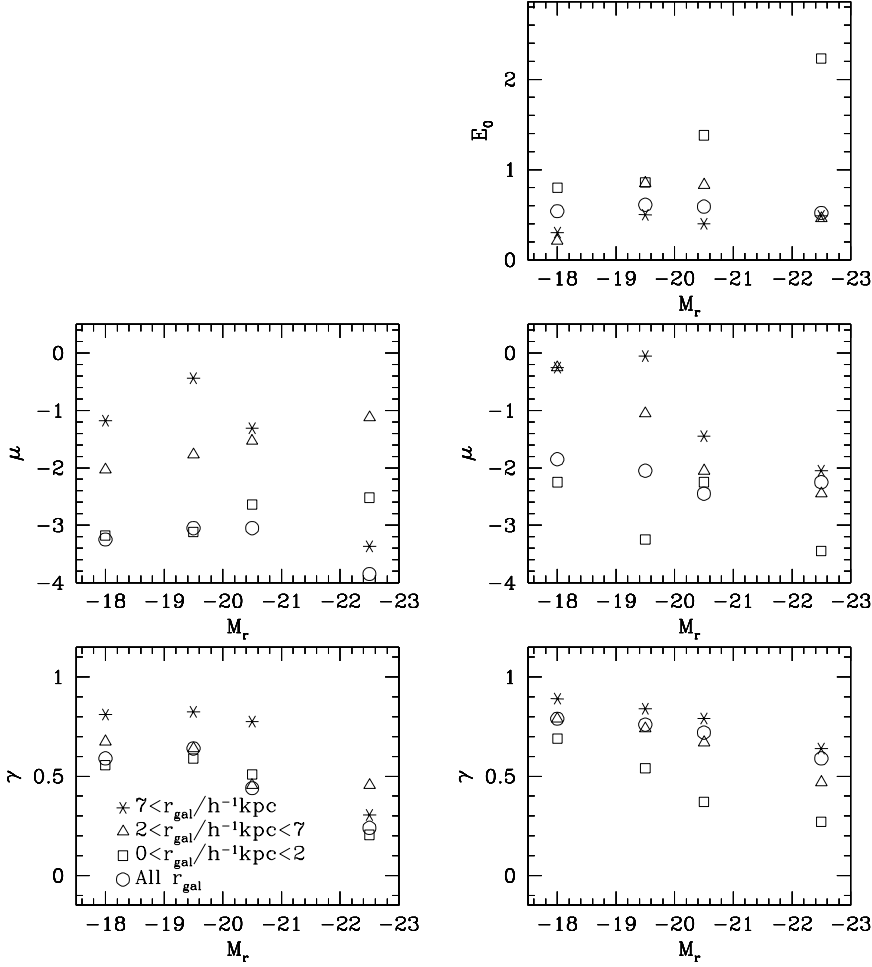


Figure 13. Best-fitting parameters as a function of galaxy luminosity for different galaxy sizes (in different symbols as shown in the figure key). Left panels correspond to elliptical galaxies, and right panels to spiral galaxies. The top panel shows the variation of the extinction, E_0 , middle panels show the mean value of μ , and bottom panels show the variation of the γ parameter.

tion of galaxies might depend on their sizes; galaxies of different sizes but similar luminosities might have different dynamical histories, and the dust column might reasonably be larger in larger galaxies.

The top panel of Figure 12 shows the dependence of the median b/a on projected galaxy size as given by the photometric model scale-length r_{gal} (exponential or de Vaucouleurs depending on the value of the fracDeV parameter). The median b/a decreases significantly for larger galaxies for both spirals and ellipticals. This effect is present at all galaxy luminosities.

With this dependence in mind, Figure 13 shows the results of fitting our model to samples of galaxies in bins of physical size at constant luminosity, where the left panels show the results for elliptical galaxies (parameters μ and γ), and the right panels for spiral galaxies (parameters μ , γ , and E_0). The best-fit parameters are presented in Table 6 for faint, spiral and elliptical galaxies, and in Table 7 for bright galaxies. At a given luminosity, small elliptical galaxies have similar model parameters as those of the full sample of ellipticals, although at high luminosity, they tend to show slightly more elongated shapes (as reflected in the μ parameter). Large elliptical galaxies, on the other

hand, are more elongated than the full sample. In particular, the $r_{gal} > 7 h^{-1} \text{ kpc}$ sample can be identified with elongated prolate shapes. Quantitatively, at low luminosities ($M_r = -18$), the median axis ratios are $B/A = 0.94$ and $C/B = 0.42$ for small galaxies, and $B/A = 0.85$ and $C/B = 0.1$ for large galaxies. We examined the SDSS images and colours of ellipticals of the most extreme axis ratio ($b/a < 0.1$); all appeared to be correctly classified.

Low-luminosity spiral galaxies, on the other hand, go from median axis ratios of $B/A = 0.86$ and $C/B = 0.2$ for small sizes to $B/A = 0.45$ and $C/B = 0.08$ for large galaxies. Thus, the disk thickness decreases with increasing size. Shao et al. (2007) assumed that μ and σ are independent of size, whereas we found that most of the changes in the shape of galaxies with size are actually absorbed by variations in these parameters. However, the conclusions of Shao et al. are robust to this detail and indicate, as our results do, that larger spiral galaxies tend to have flatter disks.

Table 6. Best fit model parameters: dependence on galaxy size for galaxies with $M_r > -19$. Small galaxies satisfy $r_{gal} < 2h^{-1}\text{kpc}$, medium galaxies, $2h^{-1}\text{kpc} < r_{gal} < 7h^{-1}\text{kpc}$, and large galaxies, $r_{gal} > 7h^{-1}\text{kpc}$.

Par.	Spirals Small	Spirals Medium	Spirals Large	Ellipticals Small	Ellipticals Medium	Ellipticals Large
E_0	0.8	0.21	0.3			
μ	-2.25	-0.25	-0.25	-3.18	-2.03	-1.18
σ	0.8	2.1	1.2	0.75	1.6	1.6
γ	0.31	0.21	0.11	0.445	0.325	0.19
σ_γ	0.07	0.05	0.01	0.17	0.17	0.05

Table 7. Best fit model parameters: dependence on galaxy size for galaxies with $M_r < -21$. Small, medium and large galaxies are selected as in table 6.

Par.	Spirals Small	Spirals Medium	Spirals Large	Ellipticals Small	Ellipticals Medium	Ellipticals Large
E_0	2.23	0.46	0.49			
μ	-3.45	-2.45	-2.05	-2.52	-1.12	-3.37
σ	0.65	0.45	0.7	2.7	2.6	0.85
γ	0.73	0.53	0.36	0.795	0.545	0.695
σ_γ	0.09	0.15	0.11	0.22	0.13	0.17

5 DISCUSSION AND CONCLUSIONS

In this paper we have addressed the problem of reproducing the observed distributions of projected axis ratios of galaxies from the SDSS. We have introduced a number of improvements over previous works including, i) the use of larger samples of galaxies made possible by the introduction of a $1/V_{max}$ weighting scheme, ii) the inclusion of the effects of dust extinction on the distribution of apparent b/a axis ratios for spiral galaxies, iii) the analysis of dependence of galaxy shapes on galaxy luminosity, colour, and physical size.

We developed a simple model for the effects of dust extinction on the distribution of apparent axis ratios and used it to constrain the intrinsic shapes of spiral galaxies. We characterise a given galaxy as a triaxial ellipsoid of axes A, B , and C from major to minor. The full sample of spiral galaxies is characterised by the mean and standard deviation of $1 - C/B$ of $\mu = -1.85 \pm 0.15$ and $\sigma = 1.04 \pm 0.19$; the distribution of $\log(1 - B/A)$ is modeled as a lognormal with mean $\gamma = 0.21 \pm 0.02$ and standard deviation $\sigma_\gamma = 0.046 \pm 0.014$. These values are in good agreement with those from the SDSS-DR1 by Ryden (2004), who finds $\mu = -1.85$ and $\gamma = 0.216$, although her widths are somewhat different from ours. More recently, Unterborn & Ryden (2008) analyse the shapes of a sample of spiral galaxies which has been corrected for the biases introduced by dust on the distribution of projected shapes. The resulting spiral shapes are characterised by $\mu = -2.56$, $\sigma = 0.91$, $\gamma = 0.216$ and $\sigma_\gamma = 0.067$, which are roughly consistent with the results we present here; however, their sample selection is explicitly dependent on their model for the dependence of dust on inclination angle, which makes it difficult to make a more quantitative comparison.

We also studied variations in the intrinsic shapes of

galaxies with galaxy luminosity (Table 4), colour (Table 5), and physical size (Tables 6 and 7). As luminosity and colour are correlated, and in particular more luminous spiral galaxies show larger bulges, we find rounder spiral galaxies at larger luminosities and $g - r$ colours. At a given luminosity, larger galaxies tend to be flatter.

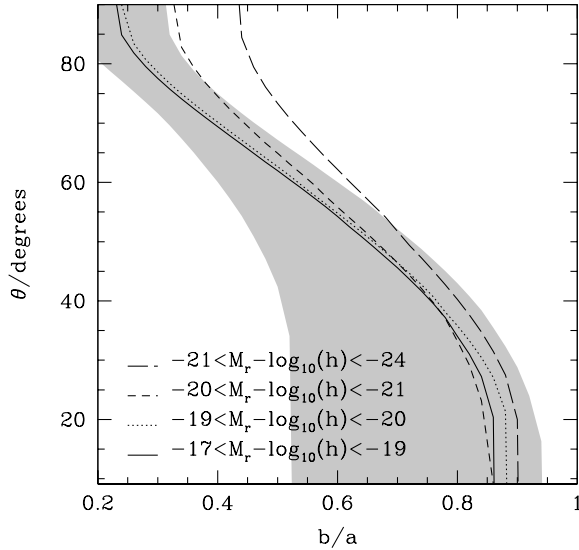
Our quoted parameters are obtained by marginalising over the extinction parameter, E_0 . The extinction is not well-constrained by the axis-ratio distribution alone, but for our full sample, we find a value $E_0 = 0.51 \pm 0.27$ after marginalising over other parameters, in good agreement with results from the literature.

Using our results from Table 4, we determine the relation between the observed projected axis ratios of spiral galaxies and the inclination angles of their disks for four different luminosity ranges. In order to do this, we simply calculate $(b/a)_{max}$ at which the distribution of projected axis ratios peaks, as well as the 10% and 90% percentiles, for a given narrow range of viewing angles. We use the percentiles to infer the range of angles that correspond to a given b/a ratio that can be measured from a spiral galaxy. Figure 14 and Table 8 show the relation between projected axis ratio b/a and polar viewing angle θ for spiral galaxies of different luminosities. The shaded area shows the ranges of polar viewing angles that correspond to a given value of b/a for the fainter sample. As brighter galaxies tend to have thicker disks, the value of b/a corresponding to edge-on bright galaxies is higher than for fainter galaxies. Note that these results take into account the effects of dust extinction.

The axis ratio distribution of elliptical galaxies shows no dependence on colour, suggesting that dust extinction is not important for this sample, and we do not include it in our modelling. The full sample of elliptical galaxies are characterised by parameters $\mu = -2.2 \pm 0.2$, $\sigma = 1.4 \pm 0.10$, $\gamma = 0.57 \pm 0.06$ and $\sigma_\gamma = 0.21 \pm 0.02$, which correspond

Table 8. Relation between b/a and polar viewing angle, θ , for subsamples of spiral galaxies corresponding to different ranges of absolute magnitude

θ degrees	b/a $\langle M_r \rangle = -18.0$	b/a $\langle M_r \rangle = -20.1$	b/a $\langle M_r \rangle = -21.2$	b/a $\langle M_r \rangle = -22.7$
3	0.8707	0.8959	0.8523	0.9134
7	0.8704	0.8956	0.8524	0.9131
11	0.8694	0.8944	0.8521	0.912
15	0.8681	0.8926	0.8502	0.9089
19	0.8629	0.8863	0.8477	0.9025
23	0.8533	0.8742	0.8404	0.8916
27	0.8413	0.8604	0.8286	0.8824
31	0.8204	0.8366	0.8115	0.8627
35	0.7931	0.807	0.7936	0.8386
39	0.7648	0.7723	0.7657	0.8098
43	0.7268	0.7375	0.7322	0.7776
47	0.6844	0.694	0.6945	0.7423
51	0.6382	0.6474	0.6533	0.7049
55	0.5921	0.5976	0.6095	0.6715
59	0.5397	0.5458	0.5677	0.6315
63	0.4859	0.4954	0.5216	0.5921
67	0.4318	0.4417	0.4754	0.5541
71	0.3788	0.3888	0.434	0.5186
75	0.3287	0.3394	0.3954	0.4875
79	0.285	0.2959	0.3629	0.4623
83	0.2512	0.2625	0.3389	0.4442
87	0.2321	0.2437	0.3261	0.4349

**Figure 14.** Relation between the polar viewing angle, θ , and projected axis ratios, b/a , for subsamples of spiral galaxies of different absolute magnitudes. The shaded area encloses 80% of the possible viewing angles associated with a given value of b/a .

to slightly oblate spheroids in agreement with results by Vincent & Ryden (2005). More luminous ellipticals tend to be rounder, although ellipticals are oblate at all luminosities. Although Vincent & Ryden (2005) found that the lowest luminosity ellipticals are best fitted by prolate spheroids, their inferred C/A axis ratio is consistent with our estimates. This work presented the most detailed statistical study

of shapes of galaxies separated in spirals and ellipticals to date, and includes the effects of dust on the distribution of projected shapes of spirals in a self-consistent way. It is remarkable that dust can be inferred from the distribution of projected axis ratios alone, although only at a low statistical significance. The dependence of intrinsic galaxy shapes and extinction with luminosity, colour and size expands the range of tests that galaxy formation models need to satisfy, to continue improving the modelling of the processes that drive the evolution of galaxies.

ACKNOWLEDGMENTS

This work was supported in part by the FONDAP “Centro de Astrofísica” and Fundación Andes. NP was supported by a Proyecto Fondecyt Postdoctoral no. 3040038 and Regular No. 1071006, and MAS was supported by NSF grants AST-0307409 and AST-0707266. We have benefited from helpful discussions with Diego García Lambas and Jeremiah P. Ostriker.

Funding for the SDSS and SDSS-II has been provided by the Alfred P. Sloan Foundation, the Participating Institutions, the National Science Foundation, the U.S. Department of Energy, the National Aeronautics and Space Administration, the Japanese Monbukagakusho, the Max Planck Society, and the Higher Education Funding Council for England. The SDSS Web Site is <http://www.sdss.org/>.

The SDSS is managed by the Astrophysical Research Consortium for the Participating Institutions. The Participating Institutions are the American Museum of Natural History, Astrophysical Institute Potsdam, University of Basel, University of Cambridge, Case Western Reserve Uni-

versity, University of Chicago, Drexel University, Fermilab, the Institute for Advanced Study, the Japan Participation Group, Johns Hopkins University, the Joint Institute for Nuclear Astrophysics, the Kavli Institute for Particle Astrophysics and Cosmology, the Korean Scientist Group, the Chinese Academy of Sciences (LAMOST), Los Alamos National Laboratory, the Max-Planck-Institute for Astronomy (MPIA), the Max-Planck-Institute for Astrophysics (MPA), New Mexico State University, Ohio State University, University of Pittsburgh, University of Portsmouth, Princeton University, the United States Naval Observatory, and the University of Washington.

REFERENCES

- Abazajian, K. et al. 2003, AJ, 126, 2081.
 Abazajian, K. et al. 2004, AJ, 128, 502.
 Abazajian, K. et al. 2005, AJ, 129, 1755.
 Adelman-McCarthy, J. et al. 2007, ApJS, in press (arXiv:0707.3413)
 Andersen, D.R. & Bershadsky, M.A. 2003, ApJ, 599, 79.
 Andersen, D.R. et al. 2001, ApJ, 551, 131.
 Bacon, R. et al. 2001, MNRAS, 326, 23
 Bak, J., & Statler, T.S. 2000, AJ, 120, 110
 Benacchio, L., & Galletta, G. 1980, MNRAS, 193, 885.
 Bernstein, G. M., & Jarvis, M. 2002, AJ, 123, 583
 Bertola, F. & Capaccioli, G. 1975, ApJ, 200, 439.
 Binggeli, B. 1980, A&A, 82.
 Binney, J.J. 1976, MNRAS, 177, 19
 Binney, J.J. 1985, MNRAS, 212, 767.
 Binney, J.J. & Merrifield, S.D. 1998, Galactic Astronomy (Princeton University Press, Princeton)
 Binney, J.J., & de Vaucouleurs, G. 1981, MNRAS, 194, 679.
 Blanton, M., & Roweis, S. 2007, AJ, 133, 734.
 Blanton, M., et al. 2003a, ApJ, 592, 819.
 Blanton, M., et al. 2003b, ApJ, 594, 186.
 Blanton, M., et al. 2005, AJ, 129, 2562.
 Burstein, D., Haynes, M., & Faber, S. 1991, Nature, 353, 515.
 Calzetti, D. 2001, PASP, 113, 1449.
 Choloniewski, J. 1991, MNRAS, 250, 486.
 Davies, R., & Burstein, D., editors, 1995, *The Opacity of Spiral Disks*, NATO ASI Series C (Dordrecht: Kluwer)
 Davies, R.L., Phillips, M., Boyce, P., & Disney, M. 1993, MNRAS, 260, 491.
 Davies, R.L., Efstathiou, G., Fall, S. M., Illingworth, G.D., & Schechter, P.L. 1983, ApJ, 266, 41.
 de Vaucouleurs, G. 1948, AnAp, 11, 247.
 de Vaucouleurs, G. & de Vaucouleurs, A. 1964, ApJ, 140, 1622.
 de Zeeuw, P.T. et al. 2002, MNRAS, 329, 513
 Ebner, K., Davis, M., & Djorgovski, S. 1988, AJ, 95, 422.
 Fasano, G. & Vio, R. 1991, MNRAS, 249, 629.
 Franx, M., Illingworth, G., & de Zeeuw 1991, ApJ, 383, 112.
 Fukugita, M., Ichikawa, T., Gunn, J.E., Doi, M., Shimasaku, K., & Schneider, D. 1996, AJ, 111, 1748.
 Giovanelli, R., Haynes, M., Salzer, J., Wegner, G., da Costa, L., & Freudling, W. 1995, AJ, 111, 1059.
 Goudfrooij, P. 2000, ASPC, 209, 74.
 Gunn, J.E. et al. 1998, A&A, 116, 3040.
 Gunn, J.E. et al. 2006, AJ, 131, 2766.
 Holmberg E. 1958, Medd. Lund Obs., No. 136
 Holwerda, B.W., Gonzalez, R.A., Allen, R.J., & van der Kruit, P.C. 2005a, A&A, 444, 319.
 Holwerda, B. W., Gonzalez, R. A., Allen, Ronald J., & van der Kruit, P. C. 2005b, AJ, 129, 1396.
 Hubble, E. 1930, ApJ, 71, 23.
 Huizinga, J.E., & van Albada, T.S. 1992, MNRAS, 254, 677.
 Ivezić, Ž. et al. 2004, AN, 325, 383.
 Keel, W.C. & White, R.E. 2001, AJ, 122, 1369.
 Knapp, J. et al. 1989, ApJS, 117, 209.
 Krause, O., Lisenfeld, U., Lemke, D., Haas, M., Klaas, U., & Stickel, M. 2003, A&A, 402, 1.
 Lambas, D., Maddox, S. & Loveday, J. 1992, MNRAS, 258, 404.
 Leeuw, L.L., Sansom, A.E., Robson, E. I., Haas, M., & Kuno, N. 2004, ApJ, 612, 837.
 Lupton, R., Gunn, J., & Szalay, A. 1999, AJ, 118, 1406.
 Maller, A.H., Berlind, A.A., Blanton, M.R., & Hogg, D.W. 2008, ApJ (submitted), ArXiv/0801.3286.
 Nelson, P., Zaritsky, D., & Cutri, R. 1998, AJ, 115, 2273.
 Park, C., & Choi, Y. 2005, 635, L29.
 Peletier, R.F., & Willner, S.P. 1992, AJ, 103, 1761.
 Pier, J., Munn, J., Hindsley, R., Hennessy, G., Kent, S., Kent, S., Lupton, R., & Ivezić, Ž. 2003, AJ, 125.
 Rix, H., & Zaritsky, D. 1995, ApJ, 447, 82.
 Roberts, M.S., & Haynes, M. 1994, ARAA, 32, 115
 Ryden, B. 2004, ApJ, 601, 214.
 Sandage, A., Freeman, K., & Stokes, N.R. 1970, ApJ, 160, 831
 Shao, Z., Xiao, Q., Shen, S., & Mo, H. 2007, ApJ, 659, 1159.
 Skrutskie M. F. et al. 2006, AJ, 131, 1163
 Smith, J., et al. 2002, AJ, 123, 2121.
 Statler, T.S. 1994a, ApJ, 425, 458
 Statler, T.S. 1994b, ApJ, 425, 500
 Statler, T.S., & Fry, A.M. 1994, ApJ, 425, 481
 Statler, T.S., Lambright, H., & Bak, J. 2001, ApJ, 549, 871
 Stoughton, C., et al. 2002, AJ, 123, 485.
 Strauss, M., et al. 2002, AJ, 124, 1810.
 Tasca, L.A.M., & White, S.D.M. 2005, astro-ph/0507249
 Temi, P., Brighenti, F., Mathews, W. & Gregman, J. 2004, ApJS, 151, 237.
 Tucker, D. et al. 2006, AN, 328, 821.
 Tully, R.B., Pierce, M.J., Huang, J.-S., Saunders, W., Verheijen, M.A.W., & Witchalls, P.L. 1998, AJ, 115, 2264.
 Unterborn, C.T., & Ryden, B.S., 2008, ApJ (submitted), ArXiv/0801.2400.
 Valentijn, E. 1990, Nature, 346, 153.
 Valentijn, E. 1994, MNRAS, 266, 614.
 Valotto, C. & Giovanelli, R. 2004, AJ, 128, 115
 Vincent, R.A. & Ryden, B.S. 2005, ApJ, 623, 137.
 York, D. et al. 2000, AJ, 120, 1579.
 Zaritsky, D. 1994, AJ, 108, 1619.